Investigations into structure and chemistry of 1D, 2D and 3D structured vanadium oxide nanomaterials for Li-ion batteries

E. Armstrong[1], M. Osiak[1], C. Glynn[1] and C. O'Dwyer[1,2]

[1]*Department of Chemistry, University College Cork, Cork, Ireland*
[2]*Micro & Nanoelectronics Centre, Tyndall National Institute, Lee Maltings, Cork, Ireland*

Routes towards the formation of inverted opal vanadium oxide electrodes are presented. Different methods of template infiltration using an IPA diluted solution of vanadium triisopropoxide are discussed and the resulting morphologies investigated using scanning electron microscopy. The effect of different heat treatments and method of sphere removal on morphology and structure is also considered. Solvent template removal retains the hydrolysed amorphous V_2O_5 structure. Raman scattering spectroscopy identifies the degree of V_2O_5 crystallinity that results from the different heat treatments. For a thicker inverted opal formed using a polystyrene template as opposed to a monolayer PMMA template, under similar conditions a different phase of vanadium oxide is observed evident by variations in Raman scattering response.

Introduction

Rechargeable lithium ion batteries offer the high specific energies needed for the ever expanding world of portable electronics, higher than other electrochemical power sources.(1) However, the expanding range of portable devices as well as other, high power applications, such as hybrid vehicles, means there is an immediate need for a storage technology capable of providing the power density of a supercapacitor and the energy density of a battery. There is a need for new electrode materials as well as new material architectures in order to improve overall battery performance. Vanadium Pentoxide (V_2O_5) has been investigated for the last 30 years as a potential cathode material due to its layered structure and weak vanadium-oxygen bonds.(2) This gives V_2O_5 a high energy efficiency and relatively high theoretical capacity, and combined with its low cost, abundance and ease of synthesis makes it an ideal cathode material for lithium ion batteries.(3) However, its performance is greatly affected by poor electronic conductivity as well as poor structural stability caused by the influence of lithium insertion and removal, limiting its long term cycling ability.(4) The development of different nanostructures of vanadium oxide has seen to alleviate some of these issues by shortening the diffusion distance for lithium ions and allowing a high freedom for volume change during the lithium intercalation and de-intercalation processes.(5-9)

One type of nanostructure whose three-dimensional porous nature, which increases the electrolyte soakage abilities and the surface area in contact with electrolyte, has shown potential for alleviating a lot of the conductivity and volume expansion issues related to vanadium oxide, is that of inverted opal architectures.(10) A completely interconnected material maintains and in some cases improves electrical conductivity and therefore eliminates the need for other binders or conductive additives that add 'dead weight' to the battery. This, combined with the shorter diffusion distances given by the porous structure, offers the possibility of improved rate capabilities and overall performance.(11, 12) Inverted opal architectures are formed from sacrificial opal or photonic crystal templates. These

templates can be formed by the assembly of polymer or silica spheres into ordered arrays. This can be done by a number of ways,(13) such as, drop-casting,(14) spin-coating,(15) electrophoretic deposition,(16) vertical deposition,(17) Langmuir Blodgett,(18, 19) layer-by-layer assembly(20) or dip coating.(21) The voids between spheres are then infiltrated with a chosen material precursor and the spheres are removed to produce the inverted structure. The variety in the choice of template structure, precursor choice, infiltration method and processing, template removal, and other necessary modifications to enhance the functionality of the material, make this an attractive structure for electrode design for battery anodes and cathodes.

Experimental

Monolayer sphere templates were formed on gold coated silicon substrates by dip coating, poly(methylmethacrylate) (PMMA) spheres of 700 nm in diameter, prepared by the emulsion polymerization procedure described elsewhere,(22) in the presence of the surfactant sodium dodecyl sulphate. The surfactant sodium dodecyl sulphate (SDS) was added to a 5 wt% aqueous solution of spheres, at a concentration of 8 mg ml^{-1} above the theoretical critical micelle concentration (CMC) for SDS of 2.3 mg ml^{-1} (8.0 × 10-3 mol dm^{-3}). Dip coating, illustrated in Fig. 1c., was performed using a MTI Corporation PTL-MM01 Dip Coater apparatus, at a rate of 1 mm/min on gold coated silicon substrate. Briefly, a piece of silicon wafer, approximately 1 cm × 1 cm, was cleaned in argon plasma and coated with a 10 nm titanium adhesion layer and 100-150 nm gold by ion beam sputtering using an ATC Orion-5-UHV sputtering system. After cleaning, by sonication in acetone, ethanol, and rinsed with deionized water the sample was settled vertically in the solution of spheres and withdrawn at a rate of 1 mm/min.

Multi-layered templates on conductive substrates (ITO coated glass and gold coated silicon, prepared as described above) were formed by electrophoretic deposition. This was done using a solution of 0.8 ml of a 2.5 wt% aqueous solution of sulphated polystyrene spheres i.e. with a net negative mixed with 3.2 ml of ethanol (this was adjusted between deposits to ensure complete coverage of sample area). This formed ~ 4 ml of solution with 1.25% sphere concentration. To adjust the pH of the mixture to ~10, ammonium hydroxide was added to the solution. The substrate electrode, washed with acetone, IPA, ethanol and deionized water, was kept at a constant distance of 5 mm from a counter electrode of aluminium and these were kept completely in parallel. The electrophoretic deposition was carried out at 2.5 V applied for time periods ranging from 10 min to 1 hour. The templates were dried in air.

The inverted opals were prepared by direct infiltration of the opal templates by several methods. The precursor was formed from a mixture of IPA, deionized water, and Vanadium Triisopropoxide ($OV(OCH(CH_3)_2)_3$). The isopropanol was mixed with deionized water in the ratio of 100:0.1 and then vanadium triisopropoxide was added to this IPA and water solution in the ratio of 100:1. This precursor was then directly applied to the opal templates and these were then followed by a treatment through calcination and/or crystallization in a furnace or by UV-ozone treatment.

Characterization of the opal and inverted opal templates were performed using scanning electron microscopy (SEM), performed on a Hitachi S-4800 field emission SEM, and this was used to visualize the in-plane (top layer) ordering of the samples. Raman scattering spectroscopy was performed using a Renishaw InVia Raman Spectrometer with a 514 nm 30mW argon ion laser and spectra were collected using a RenCam CCD camera. The beam was focused onto the samples using a 50× objective lens.

Results and discussion

Figure 1a outlines the template formation by electrophoretic deposition of the PS spheres onto ITO glass. The resulting polymer sphere deposit can be observed in Fig. 1b. The (111) plane forms preferentially to other planes due to the spheres having the lowest energy (maximum packing) in this arrangement and the (111) face is clearly visible having formed parallel to the substrate. The thickness of the deposit can be increased by lengthening the time of deposition but it is probable that eventually the deposited spheres will begin to screen the charge from the electrode and weaken the attractive forces induced on the negatively charged spheres.(23)

A similar (111) surface is visible on the monolayer PMMA templates formed at the rate of 1 mm/min on the gold substrates by dip-coating. The fast rate coupled with the gold surface, that has quickly turned hydrophobic by the interaction with carbonaceous contamination,(24) causes only a single monolayer of PMMA spheres to deposit. This monolayer of PMMA spheres is seen to scatter light in the visible range, similar behaviour to that of a two-dimensional (2D) diffraction grating. This can be used as an indication of the level of 2D order present in the sample. SEM shows evidence of some local distortions in the films, likely due to poor particle size distribution and the shrinkage of the spheres during drying. This cracking due to shrinkage is particularly prevalent in self-assembly systems involving a large volume fraction of water.

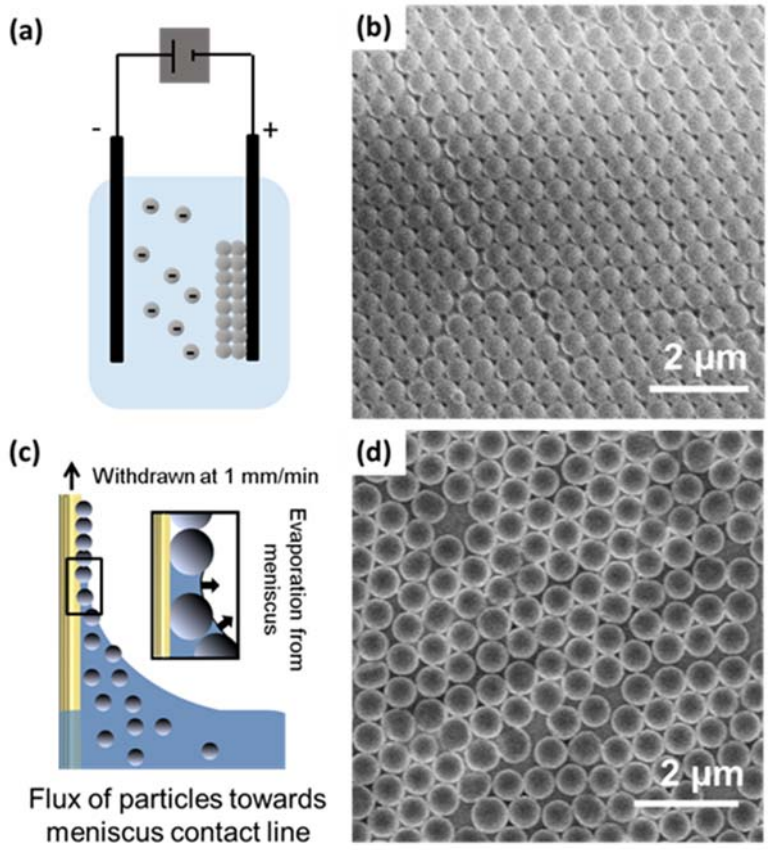

Figure 1. (a) Schematic diagram depicting EPD deposition (b) SEM image of polystyrene spheres forming opal template after EPD deposition of 10 min on ITO glass substrate (c) Schematic diagram depicting dip-coating of the PMMA spheres (d) SEM image of a monolayer of PMMA spheres formed on gold coated silicon by dip-coating.

Infiltration of the precursor was performed after the template preparation. A variety of methods were attempted with the objective of obtaining a vanadium oxide inverted opal that maintains the order and structural integrity of the template. For comparison, pre-mixing of dried PMMA spheres with the 100:1:0.1 (IPA: $OV(OCH(CH_3)_2)_3$: deionized water) precursor i.e. using no pre-made template, was also investigated. The complete mixture was then centrifuged, dried and calcined at 450°C for 5 h. The high temperature of the template removal accelerates and finalizes the process of hydrolysis of the vanadium oxide precursor and crystallizes the amorphous vanadium oxide inverted opal. This resulted in a varied morphology with little resemblance to an ordered inverted structure, shown in Fig. 2a. When the same solution was drop cast and then calcined the resulting structure, in Fig. 2b resembled that of an inverted photonic glass, a disordered arrangement of thin-walled pores. This was done to identify the degree of order after drying of the precursor therefore forming template and material architecture simultaneously. This method is particularly beneficial where long range order in 3D is a lesser requirement to thick, higher gravimetric density materials where at least the pores size is defined.

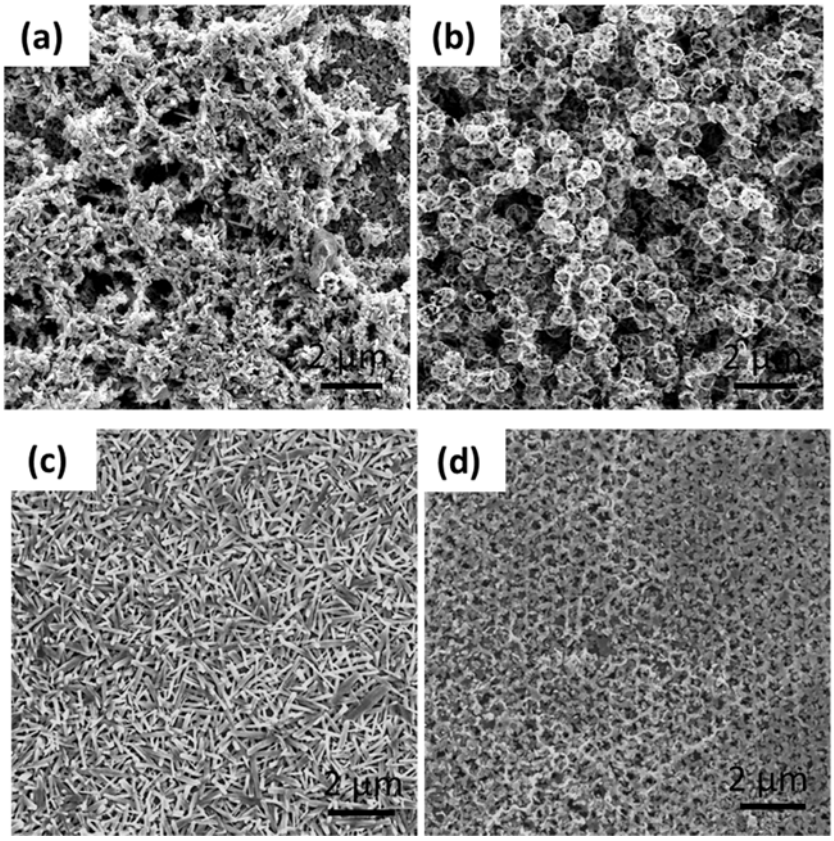

Figure 2. SEM images of inverted opals prepared by (a) centrifuging a pre-mixed PMMA sphere and precursor solution (b) Drop casting a pre-mixed PMMA sphere and precursor solution (c) Drop casting the 100:1 precursor under sonication on to a PS template formed from 1 h EPD (d) Drop casting the 100:1 precursor under sonication on to a PS template formed from 10 min EPD. All structures were calcined at 450°C for 5 h.

Next the precursor solution was drop cast directly on to the already made templates while under sonication. This template was deposited using EPD for 1 h of applied voltage and another after 10 minutes. The sample was then dried in air and calcined in a furnace for 5 h at

450 °C. The resulting V_2O_5 structure, shown in Fig. 2c, comprised of rods with no visible inverted opal structure. The prevalence of characteristic rod structure of V_2O_5 is likely due to the production of a thin film over-layer that formed almost immediately on the surface of the opal template due to hydrolysis of the material before complete infiltration into a thick template formed by EPD over a period of 1 h. The calcination process then caused a rapid growth of the vanadium over the template with a favoured rod formation. The thinner EPD template in Fig. 2d, showed some areas with a partial inverted structure characterized by incomplete walls.

Next another type of infiltration method was investigated, that of dip-coating, this has been shown previously as a successful method for template infiltration due to capillary interactions.(25) However, in order to avoid any infiltration issues that could arise with thicker templates, this was first done with a monolayer opal template. A PMMA monolayer template was dip coated in the precursor solution and removed at a rate of 200 mm/min. The process was repeated 10 times and the sample subsequently heated at 300 °C for 12 h in order to slowly crystallize the material; the resulting structure is shown in Fig. 3a comprising crystalline V_2O_5-coated spheres. For comparison, a multilayer PS opal template formed after EPD for 10 min was then dip-coated at the same rate of 200 mm/min (repeated ×10) and heated for 12 h at 300°C. After heat treatment, this sample showed an inverted opal structure shown in Fig. 3b.

In order to assess the crystal structure after calcination, Raman scattering measurements were performed on the vanadium oxide opal and inverted opal-type structures shown in Figs 3a and b. Remarkably, for the structure in Fig. 3a, we find evidence of crystallization of the hydrolysed precursor to crystalline V_2O_5 (orthorhombic structure of space group P*mnm* with D_{2h} point symmetry) evident by the vibrations located at approximately, 104, 146, 198, 284, 303, 404, 526, 698 and 996 cm^{-1} which can be indexed to the Raman signature for crystalline V_2O_5.(26, 27) To form an opal V_2O_5 structure (as opposed to the classical inverted opal structure formed after polymeric opal template removal), the hydrolysis step of the precursor needs to be quite fast so that the precursor solidifies in between the spheres, and also around the spheres. In such a case, it is possible that the removal of the polymer spheres leaves behind hollow spheres of V_2O_5 after heating and crystallization. However, these vibrations are slightly weaker than is usually observed for perfect crystalline vanadium oxide and will likely improve on heating for a longer time.

For the inverted opal structure formed after successive dip-coating of the thinner EPD formed opal template (Fig. 3b), Raman scattering data indicates the formation of a different crystalline phase of vanadium oxide. The peaks normally associated with crystalline V_2O_5 are not all visible and those that can be observed are of low intensity. The peak normally indicative of the long range order within the V_2O_5 planes, at 145 cm^{-1}, is not visible and the peak at 167 cm^{-1} dominates the low frequency end of the spectrum. This vibrational mode has been associated with VO_x nanotubular structures and could be considered as a characteristic of layered VO_x structure. These areas of the spectrum are compared further in Fig.4 a and b, where the differences between the two spectra are more clearly seen. It is known for V_2O_5 that under different morphologies as discussed by Su *et al.* that several growth mechanisms can occur for different morphologies of vanadium oxide which produce different vibrational responses.(28,29) The peaks at ~848 cm^{-1}, 881 cm^{-1} and 936 cm^{-1} have also been discussed as a phase found in VO_x nanotubes. In particular, the peaks at 848 and 936 cm^{-1} have been previously been assigned to a mode of VO_2.(28-32). The vibration mode representing the V=O normally located at approximately 995 cm^{-1} is not observed at this wavenumber in the sample from Fig. 3b. This is further evidence to the different phase of

vanadium oxide present in this sample. With further heating it is expected that the these peaks would disappear and the sample would crystallize to V_2O_5.(28)

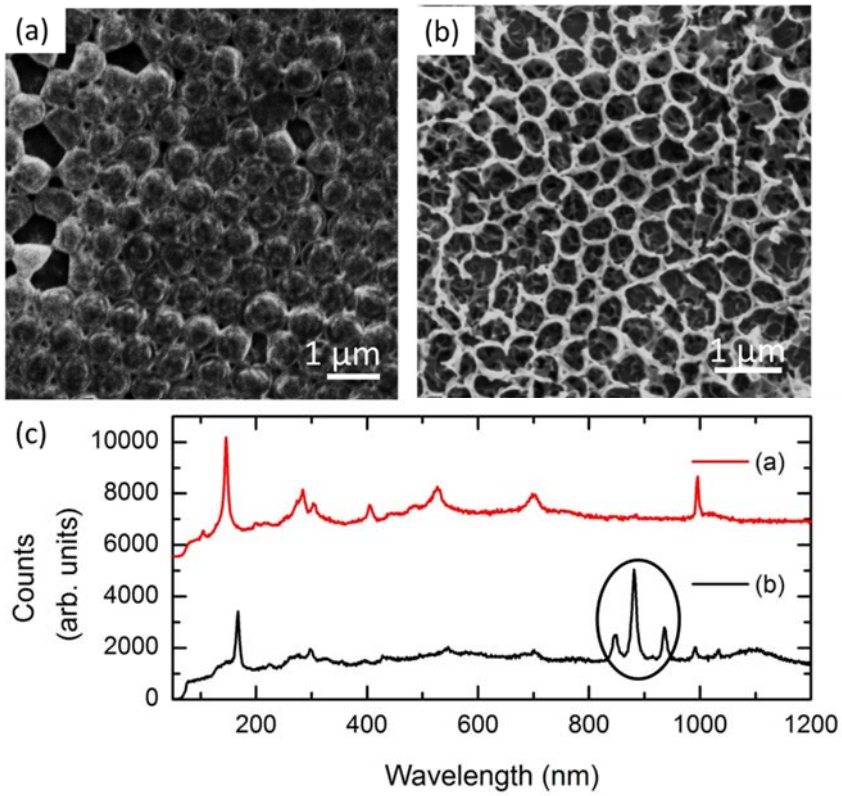

Figure 3. SEM images of (a) a monolayer PMMA template dip coated (200 mm/min × 10) and in precursor solution heated in an oven for 12 h at 300 °C and (b) multi-layer PS template dip coated (200 mm/min × 10) in precursor solution and heated at 300 °C for 12 h (c) Raman spectra for both samples confirming crystalline V_2O_5 for (a) and a different phase for (b).

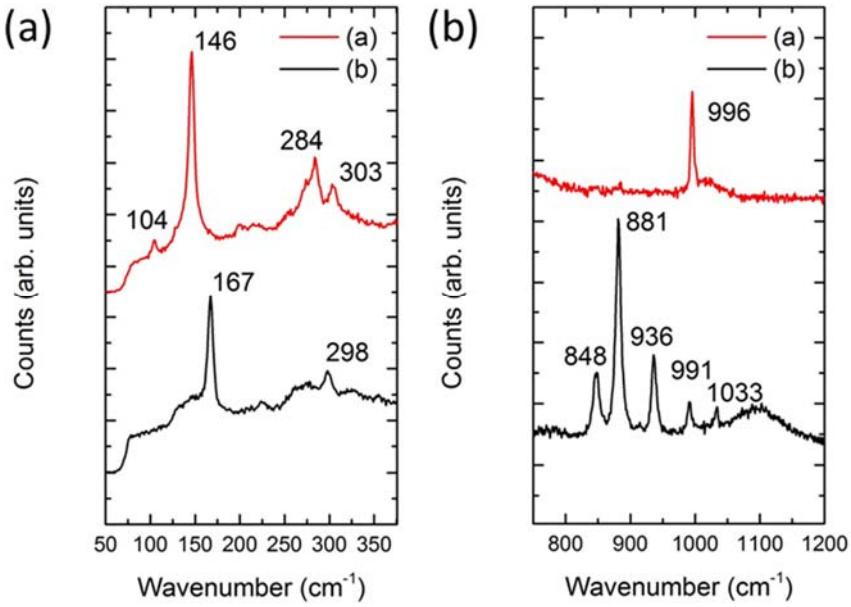

Figure 4. Magnified region of the Raman scattering spectra shown in Fig. 3c indicating the variations between the vibrations at the (a) lower frequency region and (b) higher frequency region for the two samples.

Another method for template removal is by way of solvent vapour exposure, which allows the removal of the spheres without directly affecting the material growth in the voids. Unlike the high temperature removal, an amorphous material is formed, which could then be crystallized later. A template formed after 10 min of EPD was dip coated at a rate of 200 mm/min (repeated ×10) and then submerged in toluene for 24 hours. The resulting structure is shown in Figs 4a and b. This method produced a very thin, slightly disordered structure which is most likely due to uneven filling of the template during dip coating. Therefore the removal of the spheres causes certain areas to collapse on others, disrupting the ordered pattern. However, ordered regions still exist, with smooth walls surrounding the pores. Raman scattering data shown in Fig. 4c confirm the amorphous nature of the material. Solvent vapour template removal methods offer a gentler route for thin inverted opals allowing the amorphous phase to be retained.

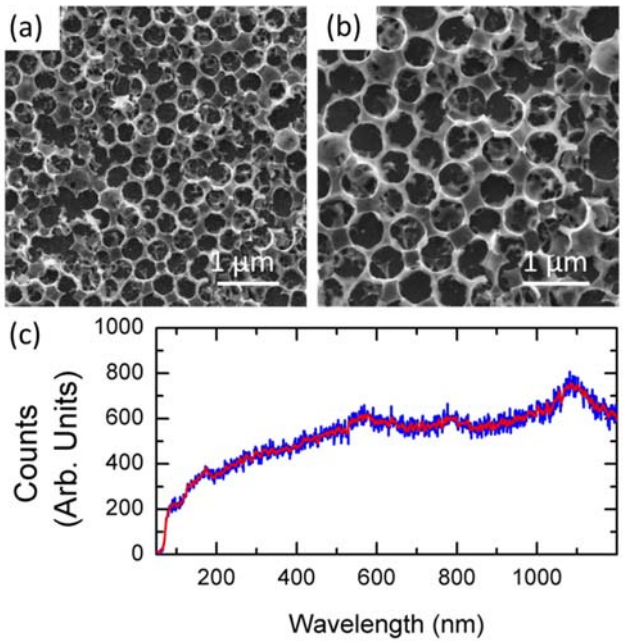

Figure 5. SEM images of a sample dip coated (200 mm/min × 10) in the precursor solution and then submerged in toluene for 24 h to dissolve the template. (b) Raman scattering measurements that confirm an amorphous vanadium oxide inverted opal.

Templates were formed using 500 nm spheres and the plot profiles across the inverted opals formed by the two methods discussed in Fig. 3b and Fig. 4 above indicate a value for the pores very close to 500 nm. Therefore, this points towards a consistency in pore size for both methods of IO formation. However, in the sample formed by heating at 300 °C for 12 hours, small peaks are visible in between the larger peaks, at an average distance of 222 nm from the pore walls. This indicates the presence of small islands between the pores. These islands could be partial remnants of the spheres or precursor that infiltrated beneath the template and pooled directly below each sphere.

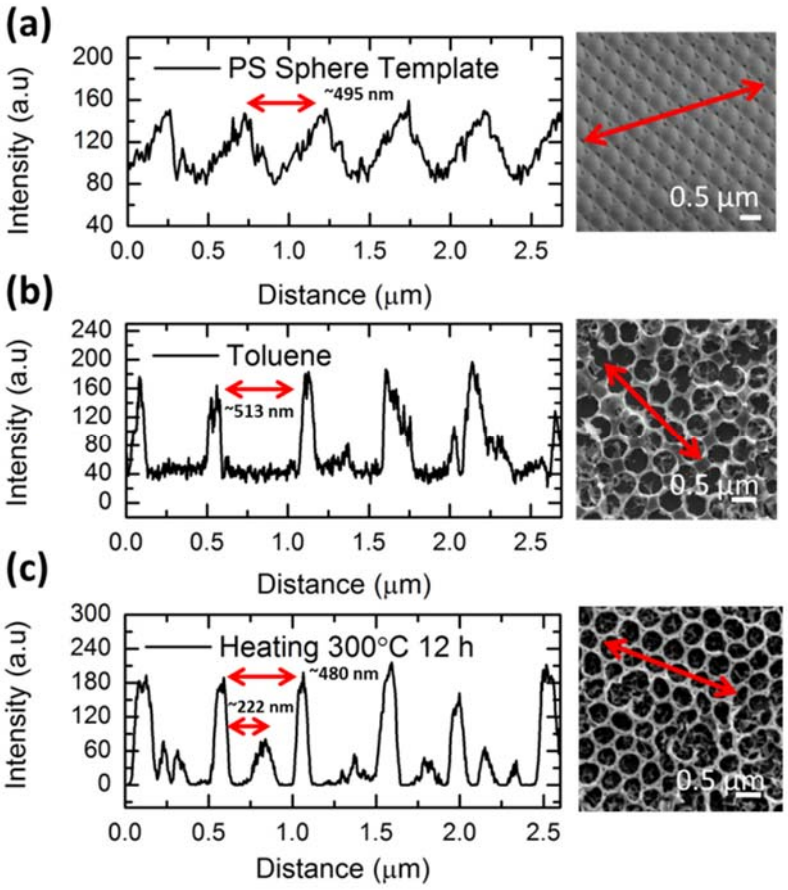

Figure 6. Line profiles from SEM images for (a) a template formed from PS spheres after EPD for 10 min indicating a sphere diameter of approximately 500 nm and (b) the sample shown in Fig. 3b indicating an average pore size of approximately 513 nm when the template is removed by toluene and (c) Fig. 4 above with an average pore size of approximately 480 nm when it is removed by heating at 300 °C for 12 h.

Compared to other infiltration methods such as CVD or electro-deposition, these infiltration methods offer the advantage of simplicity and low cost, which is desirable for up-scaled charge storage applications.

Conclusions

In summary, we prepared opal templates by two methods that of electrophoretic deposition to produce multilayer templates with 500 nm PS spheres and dip coating to produce monolayer templates of 700 nm PMMA spheres. Using these templates we then prepared inverted opal structures by a variety of methods with the aim of achieving the best structural order. We examined the formation and crystallization of the V_2O_5 through Raman scattering and showed that the type of precursor deposition and subsequent treatment and removal of the sphere template greatly influences the morphology, crystallinity and phase of the inverted opals structures formed.

Acknowledgments

EA, MO, and CG acknowledge the support of the Irish Research Council under awards RS/2010/2170, RS/2010/2920, and RS/2011/797. COD acknowledges support from Science

Foundation Ireland under award no. 07/SK/B1232a-STTF11, the UCC Strategic Research Fund, and from the Irish Research Council New Foundations Award.

References

1. K. Kang, Y. S. Meng, J. Bréger, C. P. Grey and G. Ceder, *Science*, **311**, 977 (2006).
2. M. S. Whittingham, *J. Electrochem. Soc.*, **123**, 315 (1976).
3. M. Winter, J. O. Besenhard, M. E. Spahr and P. Novák, *Adv. Mater.*, **10**, 725 (1998).
4. F. Coustier, J. Hill, B. B. Owens, S. Passerini and W. H. Smyrl, *J. Electrochem. Soc.*, **146**, 1355 (1999).
5. A. Pan, J.-G. Zhang, Z. Nie, G. Cao, B. W. Arey, G. Li, S.-q. Liang and J. Liu, *J. Mater. Chem.*, **20**, 9193 (2010).
6. C. R. Sides and C. R. Martin, *Adv. Mater.*, **17**, 125 (2005).
7. Y. Wang, K. Takahashi, K. Lee and G. Z. Cao, *Adv. Funct. Mater.*, **16**, 1133 (2006).
8. M. Zeng, H. H. Yin and K. Yu, *Chem. Eng. J.*, **188**, 64 (2012).
9. S. Q. Wang, S. R. Li, Y. Sun, X. Y. Feng and C. H. Chen, *Energ. Environ. Sci.*, **4**, 2854 (2011).
10. J. S. Sakamoto and B. Dunn, *J. Mater. Chem.*, **12**, 2859 (2002).
11. A. Esmanski and G. A. Ozin, *Adv. Funct. Mater.*, **19**, 1999 (2009).
12. D. L. Ma, Z. Y. Cao, H. G. Wang, X. L. Huang, L. M. Wang and X. B. Zhang, *Energ. Environ. Sci.*, **5**, 8538 (2012).
13. G. von Freymann, V. Kitaev, B. V. Lotsch and G. A. Ozin, *Chem. Soc. Rev.*, **42**, 2528 (2013).
14. N. D. Denkov, O. D. Velev, P. A. Kralchevsky, I. B. Ivanov, H. Yoshimura and K. Nagayama, *Langmuir*, **8**, 3183 (1992).
15. M. Pichumani, P. Bagheri, K. M. Poduska, W. Gonzalez-Vinas and A. Yethiraj, *Soft Matter*, **9**, 3220 (2013).
16. A. L. Rogach, N. A. Kotov, D. S. Koktysh, J. W. Ostrander and G. A. Ragoisha, *Chem. Mater.*, **12**, 2721 (2000).
17. P. Jiang, J. F. Bertone, K. S. Hwang and V. L. Colvin, *Chem. Mater.*, **11**, 2132 (1999).
18. B. van Duffel, R. H. A. Ras, F. C. De Schryver and R. A. Schoonheydt, *J. Mater. Chem.*, **11**, 3333 (2001).
19. M. Bardosova, P. Hodge, L. Pach, M. E. Pemble, V. Smatko, R. H. Tredgold and D. Whitehead, *Thin Solid Films*, **437**, 276 (2003).
20. J. R. Oh, J. H. Moon, S. Yoon, C. R. Park and Y. R. Do, *J. Mater. Chem.*, **21**, 14167 (2011).
21. A. S. Dimitrov and K. Nagayama, *Langmuir*, **12**, 1303 (1996).
22. R. C. Schroden and N. Balakrishnan, *Inverse Opal Photonic Crystals: A Laboratory Guide*, University of Minnesota Materials Research Science and Engineering Center, University of Minnesota,Amundson Hall 491,421 Washington Ave. SE, Minneapolis, MN 55455 (2001).
23. J. J. Van Tassela and C. A. Randall, *Key Eng. Mater.*, **314**, 167 (2006).
24. T. Smith, *J. Colloid Interface Sci.*, **75**, 51 (1980).
25. Y. Fu, Z. Jin, Z. Liu and W. Li, *J. Euro. Ceram. Soc.*, **27**, 2223 (2007).
26. X. J. Wang, H. D. Li, Y. J. Fei, X. Wang, Y. Y. Xiong, Y. X. Nie and K. A. Feng, *Appl. Surf. Sci.*, **177**, 8 (2001).
27. R. Baddour-Hadjean, E. Raekelboom and J. P. Pereira-Ramos, *Chem. Mater.*, **18**, 3548 (2006).

28. Q. Su, C. K. Huang, Y. Wang, Y. C. Fan, B. A. Lu, W. Lan, Y. Y. Wang and X. Q. Liu, *J. Alloys Compd*, **475**, 518 (2009).
29. C. O'Dwyer, V. Lavayen, M. A. S. Ana, E. Benavente, G. González and C. M. S. Torres, *J. Electrochem. Soc.*, **154**, K29 (2007).
30. E. Armstrong, W. Khunsin, C. M. Sotomayor Torres, M. Osiak and C. O'Dwyer, *ECS Trans*., **58**, ibid. (2013).
31. X. Liu, C. Huang, J. Qiu and Y. Wang, *Appl. Surf. Sci.*, **253**, 2747 (2006).
32. J. Huotari, J. Lappalainen, J. Puustinen and A. Lloyd Spetz, *Sens. Actuators B: Chemical*, **187**, 386 (2013).